materials

MDPI

Article

Effects of TiB_2 Particles on the Microstructure Evolution and Mechanical Properties of B_4C/TiB_2 Ceramic Composite

Haiyan Niu [1], Yu Zhu [2,3], Ning You [1], Yangwei Wang [3,4,*], Huanwu Cheng [3,4], Dujun Luo [3], Mengying Tang [3] and Jiamin Zhang [3]

1 Science and Technology on Complex and System Simulation Laboratory, Beijing 100072, China; niuzjs@126.com (H.N.); ningyou2021@126.com (N.Y.)
2 Beijing Institute of Aerospace Control Devices, Beijing 100039, China; 1055480577@163.com
3 School of Materials Science and Engineering, Beijing Institute of Technology, Beijing 100081, China; chenghuanwu@bit.edu.cn (H.C.); dujun2184@163.com (D.L.); tangmengying1996@163.com (M.T.); zhangjiamin1996@163.com (J.Z.)
4 National Key Laboratory of Science and Technology on Materials under Shock and Impact, Beijing 100081, China
* Correspondence: wangyangwei@bit.edu.cn

Abstract: B_4C/TiB_2 ceramic composites reinforced with three size scales (average particle size: 7 μm, 500 nm, and 50 nm) of TiB_2 were prepared by using a pressureless sintering furnace at 2100 °C under Ar atmosphere for 60 min. The results demonstrated that during the sintering process, TiB_2 located on the boundaries between different B_4C grains could inhibit the grain growth which improved the mass transport mechanism and sintering driving force. A semi-coherent interface between B_4C and SiC was found, which is supposed to help to reduce the interface energy and obtain good mechanical properties of the B_4C/TiB_2 ceramic composite. On sample cooling from sintering temperature to room temperature, the residual tensile stress fields formed at the TiB_2 interfaces owning to the thermo-elastico properties mismatched, which might have contributed to increase the ability of the sample to resist crack propagation. The results showed that the relative density, Vickers hardness, and fracture toughness of the composite with 20 wt.% submicron and 10 wt.% nano-TiB_2 were significantly improved, which were 98.6%, 30.2 GPa, and 5.47 MPa·$m^{1/2}$, respectively.

Keywords: pressureless sintering; B_4C-TiB_2; particle size; microstructure; microstructure evolution

check for updates

Citation: Niu, H.; Zhu, Y.; You, N.; Wang, Y.; Cheng, H.; Luo, D.; Tang, M.; Zhang, J. Effects of TiB_2 Particles on the Microstructure Evolution and Mechanical Properties of B_4C/TiB_2 Ceramic Composite. *Materials* **2021**, *14*, 5227. https://doi.org/10.3390/ma14185227

Academic Editor: George Wardeh

Received: 20 July 2021
Accepted: 6 September 2021
Published: 11 September 2021

1. Introduction

Boron carbide (B_4C) ceramics are interesting structural ceramics in view of their outstanding physical and mechanical properties, especially the combination of low density and extremely high hardness which make them superior anti-ballistic materials over other armor ceramics (such as Al_2O_3, SiC) [1–3]. However, the expensive costs of B_4C ceramics fabricated through the hot isostatic pressing (HIP) method severely limits its wide application in the armor protection field [4–6]. In addition, its low self-diffusivity efficiency indicates that the sintered body could not achieve the goal of densification through the single solid-state sintering technique. Recently, numerous attempts have been made to overcome these disadvantages, such as the introduction of a second phase and sintering additives into the B_4C matrix to fabricate composites. Transition metal borides, such as TiB_2 [7,8], ZrB_2 [9,10], and HfB_2 [11], having high thermal expansion coefficients, and the residual stress fields between B_4C and borides rising during the cooling process possibly enhance the fracture toughness of the fabricated composites [12,13].

Recently, the B_4C/TiB_2 ceramic composites have been the object of numerous works [14–17]. The additives of TiB_2 to B_4C phase can maintain the advantages of high Vickers hardness and low density of B_4C and, in addition, inhibit the grain growth [16]. Additionally, the physical and mechanical properties of the B_4C/TiB_2 composites without

additives prepared from the B_4C and TiB_2 powder are very low. The relative density of B_4C-30 wt.% TiB_2 composites without any additives prepared via pressureless sintering was lower than 90% [18,19]. The flexural strength of the B_4C/TiB_2 ceramic composite reached 717 MPa for the hot-pressured method, which was above two times higher than those (260–361 MPa) fabricated via pressureless sintering [16]. Many researchers have used the B_4C-TiO_2-C powder mixture to prepare the B_4C/TiB_2 composites in different ways, such as the reactive pressureless sintering, hot-pressing, and pulse electric-current sintering [20,21]. Since the introduction of fine TiB_2 grains by in-situ reaction, the B_4C and TiB_2 grain size retained submicron sizes, and the mechanical property tests indicated that the prepared B_4C/TiB_2 ceramic composites achieved the excellent Vickers hardness ~39.3 GPa and flexural strength ~865 MPa, respectively [7]. B_4C with various particle sizes was introduced to fabricate B_4C/TiB_2 ceramic composites under the condition of hot pressing, and both of the B_4C and TiB_2 grains were grown compared to the raw powders after hot pressing [22]. Many studies have shown that for B_4C ceramic composites, C and Si are good sintering aids [23–27]. Carbon removes oxides (such as B_2O_3) in the B_4C raw powder, and improves the interfacial tension by the way of solid solution of carbon atoms into the boron carbide lattice, which increases the sintering driving force [23,24]. A small amount of Si in the B_4C ceramics tends to form a silicide phase, which could improve the sintering ability of B_4C [25–27].

Although hot-pressing and pulse electric current sintering can obtain high-performance composites, the equipment and production costs are high, and the product size is small. The pressureless sintering is an efficient way to fabricate B_4C/TiB_2 composites with large sizes and low costs. At present, the research on improving the performance of the B_4C/TiB_2 ceramic composites prepared under pressureless sintering conditions is relatively scattered [18,28,29], and these reports indicate that the sintering temperature and TiB_2 content have a great influence on the microstructure and density of the composite. Additionally, the research regarding the TiB_2 particle size affecting the sintering behavior of B_4C/TiB_2 ceramic composites under pressureless sintering conditions is rarely reported. In our present work, the B_4C/TiB_2 ceramic composites with 30 wt.% TiB_2 were fabricated via the pressureless sintering method from commercial B_4C raw powder with the average size of 3 μm and TiB_2 raw powder with three different size scales (7 μm, 500 nm, and 50 nm), and mixed in variable mass ratio. In addition, carbon black and silicon particles were used as sintering auxiliary components. Furthermore, the effect of TiB_2 grains on the interfaces to optimize the microstructure of the B_4C/TiB_2 composites was thoroughly investigated. This research should be beneficial to fabricate the excellent performance of B_4C/TiB_2 ceramic composite.

2. Materials and Methods

Raw materials were B_4C powder (3 μm, purity: >99.5%; Zhengzhou Songshan Boron Technology Co., Ltd., Zhengzhou, China), silicon raw powder and carbon black raw powder (submicron, purity: >99.8%, Shanghai ST-NANO Co. Ltd., Shanghai, China), and TiB_2 powder (purity: >99%; Shanghai ST-NANO Co. Ltd., Shanghai, China). Figure 1a–c show the three type morphologies of the TiB_2 raw powders. Figure 1a depicts the microtopography of micro-TiB_2 powder with average size about 7 μm. Figure 1b,c show the microtopography of submicron TiB_2 powder with average size about 500 nm and nano-TiB_2 powder with average size about 50 nm, respectively. Table 1 lists the phase composition of the three mixtures. The mixed raw powders were ball-milled in ethyl alcohol absolute with ZrO_2 balls and then dried using a rotary evaporator (R205B, Shanghai Shensheng Technology Co. Ltd., Shanghai, China). The powder mixture was pressed in a graphite die and then cold isostatic pressed (CIP, LDJ100/320–300, Sichuan Aviation Industry Chuanxi Machine Factory, Sichuan, China) to form a green body with a 50 mm diameter. The samples were processed by pressurelss sintering in a graphite crucible (FCT Systeme GmbH, Rauenstein, Germany) at 2100 °C for 60 min at a heating rate of 10 °C per minute under flowing Ar atmosphere.

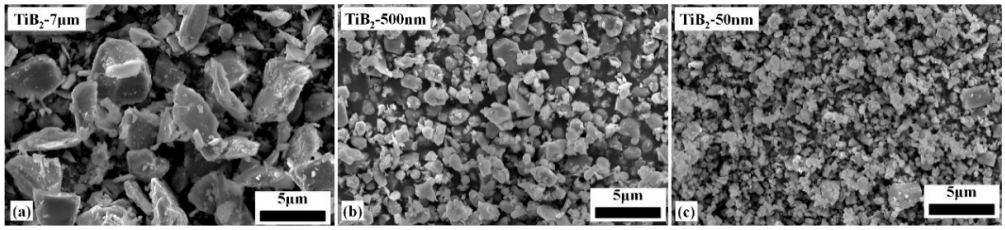

Figure 1. Nominal particle size and SEM images of commercial TiB_2 raw powders (**a**) TiB_2-7 μm (Micron), (**b**) TiB_2-500 nm (Submicron), (**c**) TiB_2-50 nm (Nano).

Table 1. Starting composition of BM30, BM10S20, and BS20N10 ceramic composites.

Grade	B_4C (wt.%)	C (wt.%)	Si (wt.%)	Micron TiB_2 (wt.%)	Submicron TiB_2 (wt.%)	Nano TiB_2 (wt.%)
BM30	60	7	3	30	/	/
BM10S20	60	7	3	10	20	/
BS20N10	60	7	3	/	20	10

The relative densities of the samples were determined through Archimedes' principle in deionized water. The average grain size was estimated by intercept method and more than 200 grains on the surface after polishing and thermally etching were measured. The flexural strength of the prepared specimens which were cut into the bars of $3 \times 4 \times 35$ mm^3 was tested on an electromechanical universal testing machine (INSTRON-5566, Norwood, MA, USA) of which the crosshead speed was 0.5 mm per minute and the span was 30 mm. The fractural toughness of the composites tested on bars (the size of $3 \times 6 \times 35$ mm^3), and a notch depth of 3 mm, was measured by the single-edge notched beam (SENB) test of which the crosshead speed was 0.05 mm per minute and the span was 24 mm. Vickers hardness measurement applied a load of 1 kg for 15 s to the sample surfaces on a hardness testing device (AHVD-1000, Shanghai Jujing Precision Instrument Manufacturing Co., Ltd., Shanghai, China). The phases and components were characterized by X-ray diffraction (D8 Advance, Germany). The microstructure was analyzed by a scanning electron microscope (SEM, Hitachi-S3400N, Hitachi, Tokyo, Japan) and a transmission electron microscope (TEM, Oxford INCAX-ACT, Oxford Instruments, Oxford, UK). The TEM sample of a selected specimen was prepared through conventional mechanical thinning and finished with precision ion polishing system machine (PIPS, Gatan-691, Pleasanton, CA, USA).

3. Results and Discussion

The phase compositions of the sintered B_4C/TiB_2 ceramic composites with various raw powders are shown in Figure 2. All samples contained B_4C, TiB_2, SiC, and graphite. The X-ray characteristic peak patterns of the BM30 and BM10S20 were the same. With the introduction of TiB_2 nanoparticle powders, the characteristic peaks of TiB_2 changed significantly. For the BS20N20, the $2\theta = 68.206°$ characteristic peak of the TiB_2 was higher than the characteristic peak intensity of the sample BM30 and BM10S20. The well-defined peaks in the as-prepared B_4C/TiB_2 composite suggests that the TiB_2 phase has a preferred orientation in (102) and (111).

Figures 3 and 4 show the SEM pictures of the fractured surface of the microstructure of the B_4C/TiB_2 ceramic composites. It could be clearly seen that due to the fact that the BM30 raw material powder particles are coarse and the sintering driving forcing is small, as shown in Figure 3a,b, there were a large number of interconnected open pores, and the coarsened particles were connected in an island chain. A large amount of sinter-necks with clear contours among the grains in the BM30 sample were still visible. With the size of TiB_2 powder decreasing, the pore content and pore size decreased, and the dense areas increased significantly, as shown in Figure 3c,f. In the BS20N10 sample containing both 500 nm and 50 nm particle sizes of TiB_2 powder, the shapes of the pores were relatively regular, tending to form regular polygon or nearly circular shapes, as shown in Figure 4a,b. Additionally, it can be inferred that these small particles belong to TiB_2.

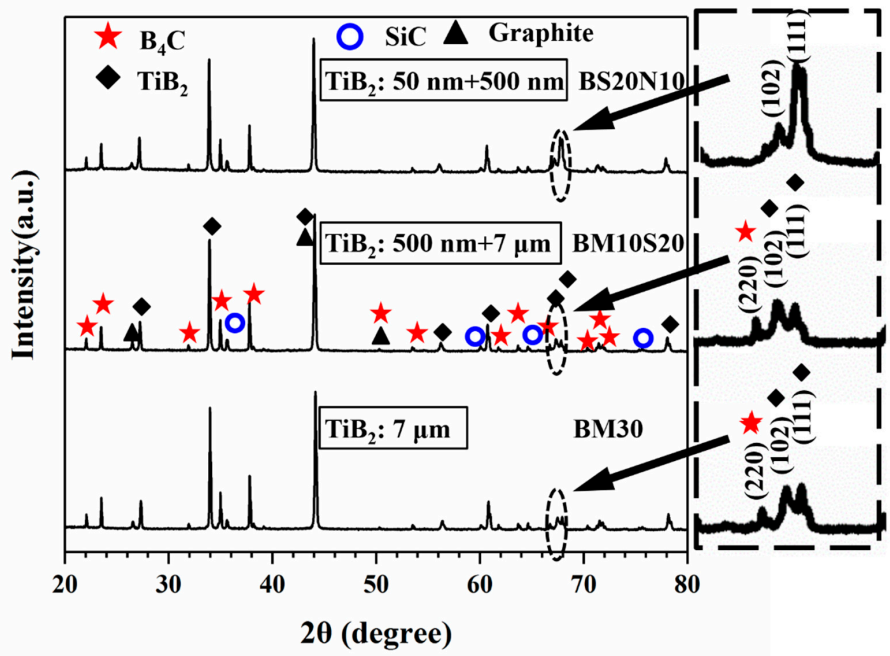

Figure 2. XRD patterns of B_4C/TiB_2 ceramic composites obtained with different grades of TiB_2 powders.

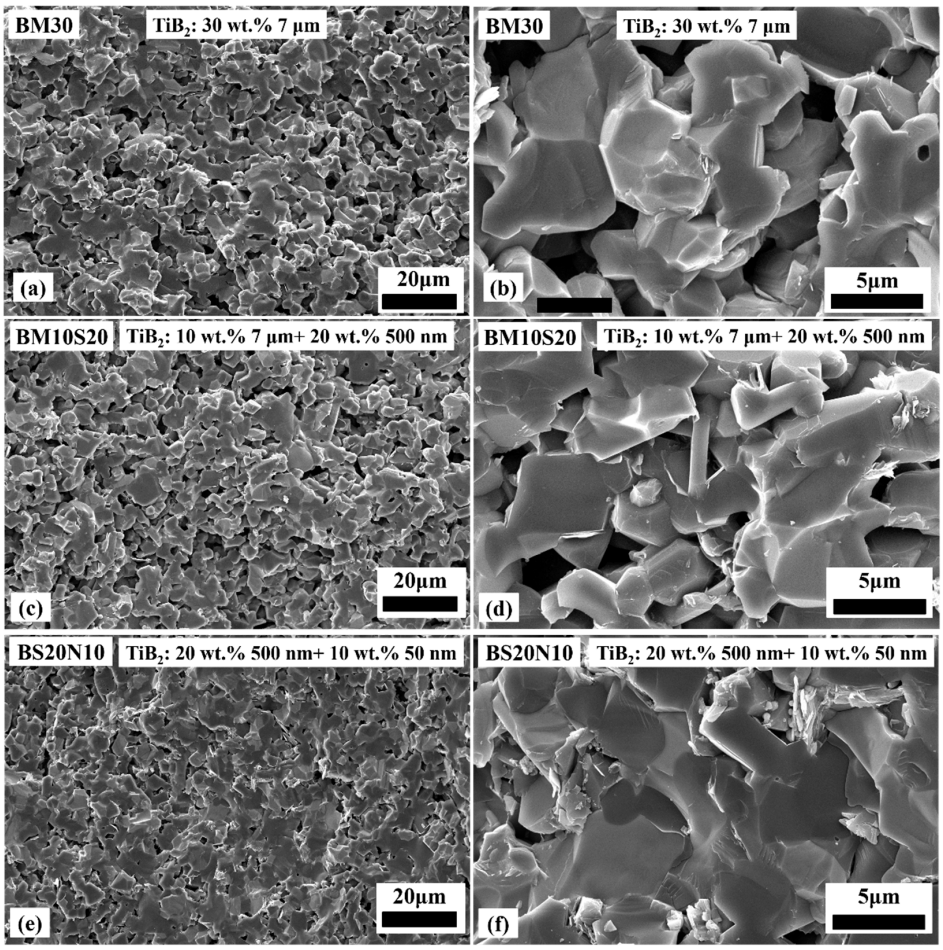

Figure 3. Fracture morphology SEM images of the B_4C/TiB_2 ceramic composites with various TiB_2 raw powder mixtures. (**a**,**b**) BM30, (**c**,**d**) BM10S20 and (**e**,**f**) BS20N10.

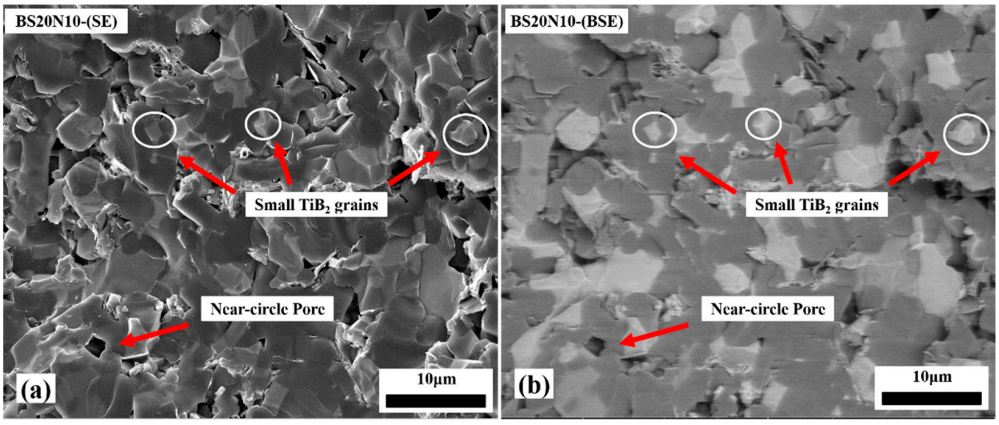

Figure 4. Small TiB_2 grains in the B_4C/TiB_2 ceramic composite processed with a mixture of sub-micron and nano-sized TiB_2 particles. (**a**) SEM image and (**b**) corresponding BSE image.

The TiB_2 grains on the grain boundaries can pin the movement of the B_4C grain boundaries and hinder the grain growth, thus increasing the content of grain boundaries and increasing the sintering rate [29]. In the BS20N10 sample, the interfaces between TiB_2 and B_4C phases are well distributed, indicating that TiB_2 and other phases achieved good wetting during the sintering process as shown in Figure 5. The interface between B_4C and TiB_2 is jagged, which indicates that the interface feature helps to improve the ability to resist external loads.

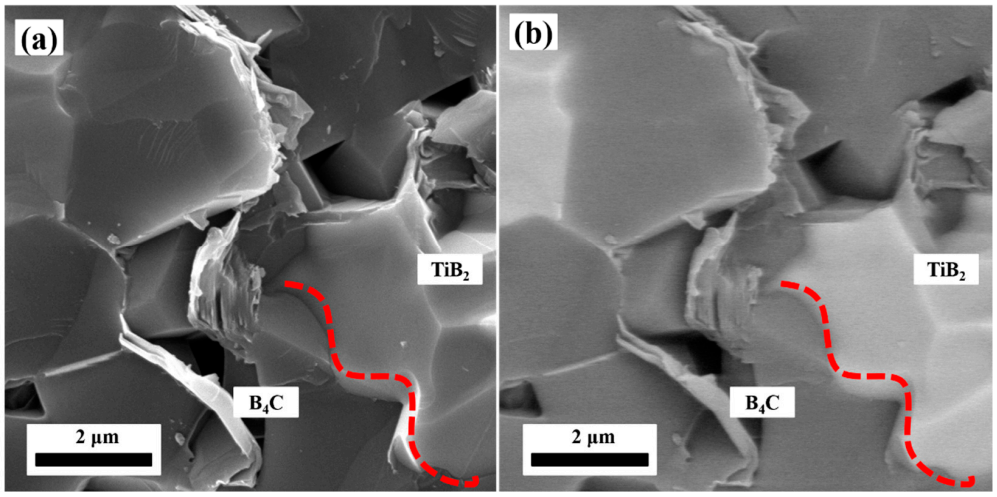

Figure 5. Interface between B_4C and TiB_2. (**a**) SEM image and (**b**) corresponding BSE image.

The SEM pictures of the polished surfaces of the specimens sintered with various TiB_2 powders are shown in Figures 6 and 7. In Figure 6, SiC grains were dispersed and distributed on the B_4C substrate in sample BS20N10, which acts as a pinning to prevent the grain boundary and inhibit grain growth. Additionally, the compound reaction of Si and C generated SiC exotherm, which helps the sintering process. Figure 7 show that the average grain sizes of the TiB_2 in the prepared specimens with various raw TiB_2 particles obtained under pressureless sintering conditions at 2100 °C for 60 min dwell were similar. B_4C grains ranged from 2 μm to 10 μm, and comparing with the TiB_2 raw powder with an average grain size of 50 nm, the grain sizes of the ceramic composites increased by a maximum of 200 times. With the size of TiB_2 raw powder decreasing, the amount and size of the pores in the samples decreased significantly. The B_4C average grain size of the BM30 sample to which the 7 μm-sized TiB_2 powder was added was 3.01 μm, but many large pores were present in Figure 7a. B_4C average grain size of the BM10S20 sample, with the

TiB_2 addition of 7 μm and 500 nm, was consistent with BM30, but the amount of the pores decreased, and the densification area of the BM10S20 sample increased. B_4C average grain size of the BS20N10 sample with the TiB_2 addition of the 500 nm and 50 nm remained close to the starting raw powder, about 2.63 μm, and the amount and size of the pores in the BS20N10 sample was significantly reduced. The relative density of the BS20N10 sample was also increased to 98.6%, as shown in Table 2.

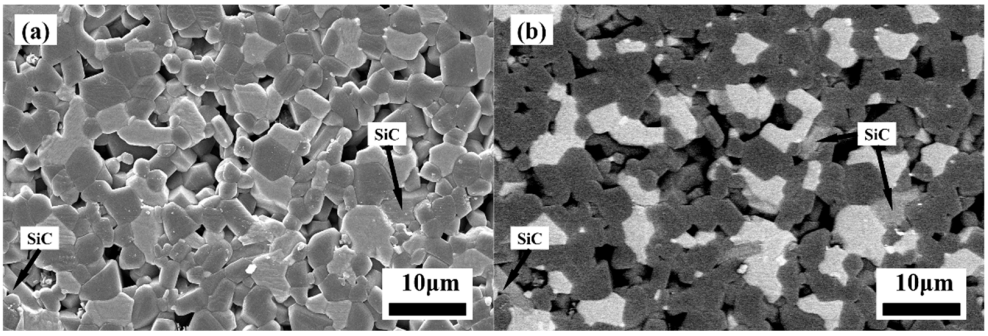

Figure 6. SEM images of the polished surfaces (**a**) and corresponding BSE images (**b**) in the sample.

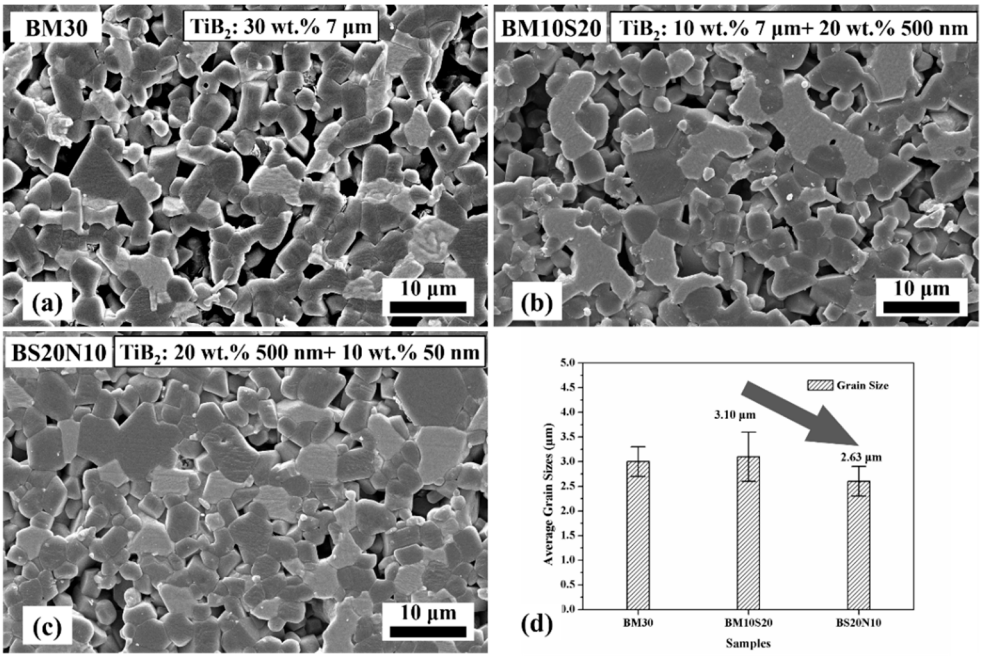

Figure 7. (**a**–**c**) SEM images of the polished surfaces and (**d**) plot of the average grain sizes in the samples.

Table 2. Mechanical properties of the B_4C/TiB_2 ceramic composites.

Sample	Relative Density (%)	Flexural Strength (MPa)	Fracture Toughness (MPa·m$^{1/2}$)	Vickers Hardness (GPa)
BM30	90.1 ± 0.2	217 ± 13	3.70 ± 0.19	8.3 ± 0.6
BM10S20	92.6 ± 0.1	288 ± 12	4.46 ± 0.12	12.5 ± 1.1
BS20N10	98.6 ± 0.1	364 ± 9	5.47 ± 0.12	30.2 ± 2.6

Figure 8a–b are TEM images of the interface structure between B_4C and SiC in the BS20N10 sample. According to the selected area-electron diffraction (SAD) result in Figure 8b, the unit cell structure parameter of B_4C was a = b = 0.56 nm, c = 1.21 nm, $\alpha = \beta = 90°$, $\gamma = 120°$, and the unit cell structure parameter of SiC was a = b = c = 0.44 nm, $\alpha = \beta = \gamma = 90°$. The zone axis of the two phases of B_4C and SiC satisfies the relationship: $[120]_{B_4C} // [\bar{1}12]_{SiC}$, and a group of

crystal planes satisfies the relationship: $(303)_{B_4C}//(311)_{SiC}$. Additionally the interface between crystal plane $(303)_{B_4C}$ and crystal plane $(311)_{SiC}$ satisfies:

$$\delta = \frac{d_{(303)} - d_{(311)}}{d_{(303)}} = \frac{0.151\text{nm} - 0.137\text{nm}}{0.151\text{nm}} = 9.27\% \quad (1)$$

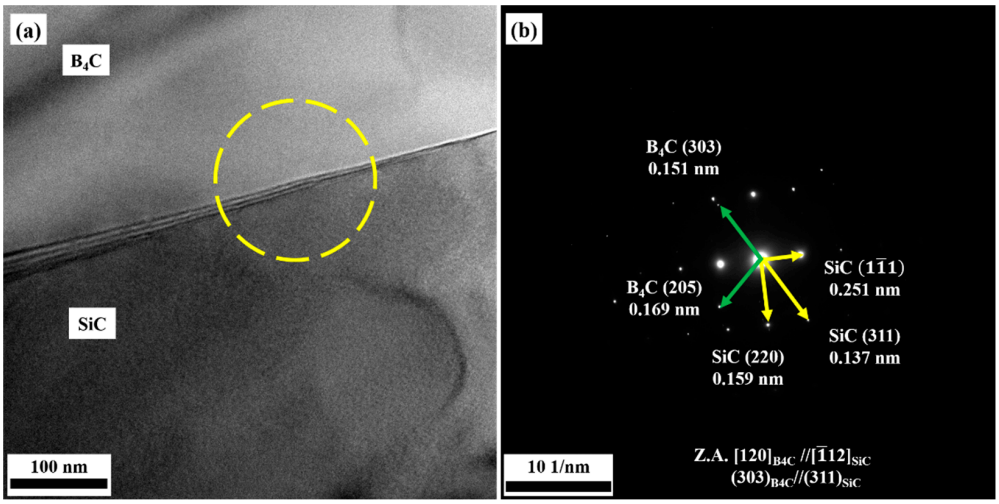

Figure 8. Interface between B_4C and SiC. (**a**) Bright field TEM image, (**b**) SAED pattern.

According to the calculation Formula (1), the mismatch degree between the crystal plane $(303)_{B_4C}$ and crystal plane $(311)_{SiC}$ is 9.27%, which could form a semi-coherent interface, and it helps to reduce the interface energy and obtains a bonding strong interface [30].

Figures 9 and 10 are the bright field and high-resolution TEM images of the interfaces between TiB_2 and B_4C, SiC, respectively. As can be seen in the bright field images of Figures 9a and 10a, the interfaces were clean and straight, and there were no other new phases. There were lattice distortion regions with a wide range of 2~3 nm at the interfaces, which were also the transition regions of the lattice structures between TiB_2 and the other two phases, shown in Figures 9b and 10b. The main reason for the formation of these transition zones may be attributed to the unit cell structure parameters of TiB_2: a = b = 0.30 nm, c = 0.32 nm, $\alpha = \beta = 90°$, $\gamma = 120°$. Additionally, the difference of the unit cell structure between B_4C, SiC, and TiB_2 was huge. During the sintering process, the transition zones were created to coordinate the arrangement of atoms at the interfaces.

The mechanical and physical properties of the prepared ceramic composites with different TiB_2 particle sizes are presented in Table 2. With the size of TiB_2 raw powder decreasing, the relative density and mechanical properties of the prepared ceramic composites all showed a significantly increasing trend. The relative density of the prepared specimens increased, which helped to achieve the excellent mechanical properties of the prepared specimens. The relative density of the BS20N10 sample reached 98.6%, which is the first major requirement to obtain competitive B_4C/TiB_2 ceramic composites. The optimized flexural strength, Vickers hardness, and fracture toughness of the BS20N10 sample reached 364 MPa, 30.2 GPa, and 5.47 MPa·$m^{1/2}$, respectively.

The relative density of the BS20N10 sample was high (98.6%) and the grain sizes were fine (about 2.63 μm), which were mainly due to the following four aspects: (1) the 50 nm-sized TiB_2 particles filled the pores of the green body and increased the density of the green body, being conducive to higher densification upon sintering; (2) with the size of the TiB_2 powder decreasing, the specific surface energy of the green body was higher than in analogous compositions with coarser grain sizes, which provides a strong driving force for sintering; (3) with the size of TiB_2 powder decreasing, the amount of the grain boundary increased, resulting in enhanced grain boundary diffusion during the sintering process;

(4) TiB_2 grains on the grain boundaries hindered the movement of the grain boundaries and helped to preserve a fine B_4C grain size.

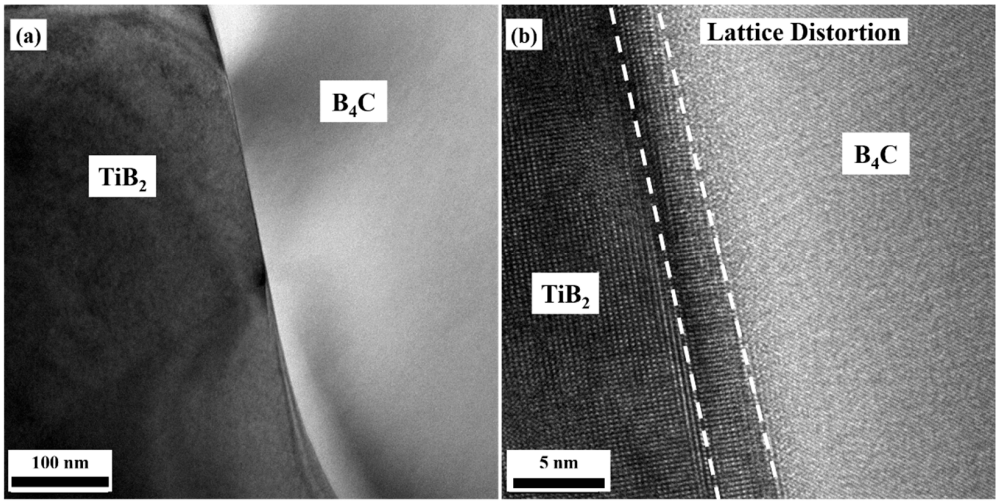

Figure 9. Interface structure between B_4C and TiB_2. (**a**) Bright field TEM image, (**b**) HRTEM image.

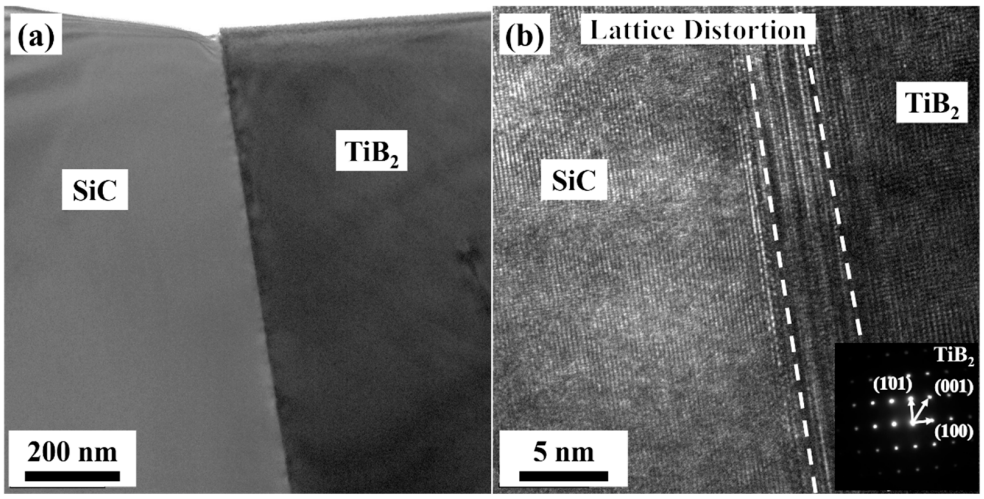

Figure 10. Interface structure between SiC and TiB_2. (**a**) Bright field TEM image, (**b**) HRTEM image.

The improvement of the relative density and reduction of the grain size of the samples both contributed to obtain high flexural strength. In addition, the shapes of the pores in the BS20N10 were regular polygons or near circles, as shown in Figure 4. According to the fracture mechanics of ceramic materials [31–33], these types of the pores could significantly increase the critical value of fracture failure caused by the stress concentration in the sample, and the sample could achieve a high flexural strength.

The thermal expansion coefficients of TiB_2 (8.1×10^{-6}/°C), B_4C (4.5×10^{-6}/°C), and SiC (4.7×10^{-6}/°C) are quite different [34,35]. During the cooling process, the residual tensile stress fields rise at the interfaces between TiB_2 and another phase (such as B_4C or SiC). When the crack enters the residual stress field zone, the crack propagated proceeds in the direction perpendicular to the tensile stress as shown in Figure 11, so that the crack propagation directions can be deflected. The crack deflections and the crack propagation paths are extended, which increase the energy consumption and increase the fracture toughness of the prepared ceramic composite.

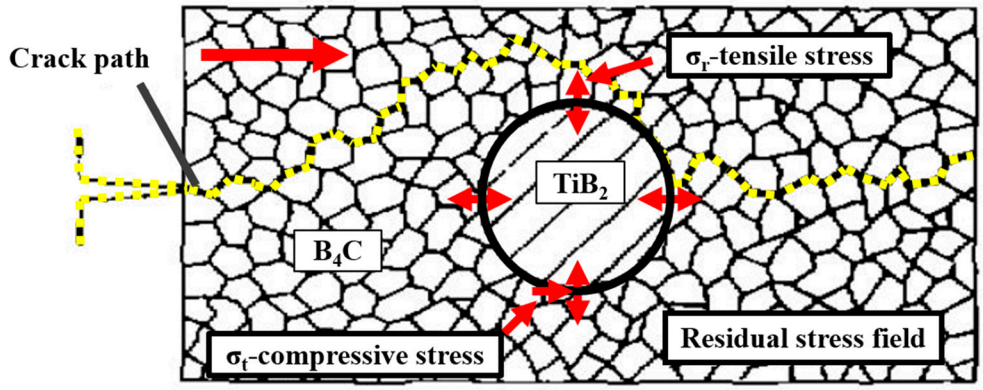

Figure 11. Schematic diagrams of the toughing mechanism by residual stress.

4. Conclusions

B_4C/TiB_2 ceramic composites containing different proportions of submicron and nano TiB_2 powders were prepared by pressureless sintering at 2100 °C. With the decrease of the particle size of TiB_2 raw powders, the surface energy of the powder increased significantly and the density of the sintered body increased. During the sintering process, nano-TiB_2 inhibited the grain growth, increased the number of the grain boundaries, and promoted the densification of the material to 98%. With the size of TiB_2 powders decreasing, the average grain sizes of the B_4C/TiB_2 ceramic composites decreased, and the interfaces between the different phases were strongly bonded, which helped to obtain good mechanical properties. As a result, the B_4C/TiB_2 ceramic composite with 20 wt.% submicron and 10 wt.% nano-TiB_2 addition had a significant improved in mechanical and physical properties. The optimized relative density, grain size, Vickers hardness, flexural strength, and fracture toughness of the sample were 98.6%, 2.63 µm, 30.2 GPa, 364 MPa, and 5.47 MPa·$m^{1/2}$, respectively. Finally, it was illustrated that the sub-fine TiB_2 powder could control the grain growth in the preparation of the B_4C/TiB_2 ceramic composite under the pressureless sintering condition, and was confirmed to be an effective approach to enhance the mechanical properties of B_4C ceramics.

Author Contributions: H.N. and Y.Z. conducted experiments and data analysis works, and H.N. and Y.Z. wrote and revised the manuscript; Y.W. and H.C. contributed to the conception of the study; N.Y., D.L., M.T. and J.Z. helped perform the pressureless sintering tests and analysis of the results. All authors have read and agreed to the published version of the manuscript.

Funding: This research received no external funding.

Institutional Review Board Statement: Not applicable.

Informed Consent Statement: Not applicable.

Data Availability Statement: Not applicable.

Acknowledgments: The authors wish to acknowledge the Beijing Centre for Physical & Chemical Analysis and Fuzhou Qiyue Micro Powder Co., Ltd. for their help in experiment work and analysis technical support.

Conflicts of Interest: The authors declare no conflict of interest.

References

1. Thevent, F. Boron Carbide—A Comprehensive Review. *J. Eur. Ceram. Soc.* **1990**, *6*, 205–225. [CrossRef]
2. Jiang, Z.G.; Zeng, S.Y.; Shen, Z.Q. Research progress on lightweight ceramic composite armor structure. *Acta Armamentarii* **2010**, *31*, 603–610. [CrossRef]
3. Karandikar, P.G.; Evans, G.; Wong, S.; Aghajanian, M.K.; Sennett, M. A review of ceramics for armor applications. *Adv. Ceram. Armor IV* **2009**, *29*, 163–175. [CrossRef]
4. Savio, S.G.; Ramanjaneyulu, K.; Madhu, V.; Bhat, T.B. An experimental study on ballistic performance of boron carbide tiles. *Int. J. Impact Eng.* **2011**, *38*, 535–541. [CrossRef]

5. Da Rocha, R.M.; de Melo, F.C.L. Pressureless Sintering of B_4C-SiC Composites for Armor Applications. *Ceram. Eng. Sci. Proc.* **2009**, *30*, 113. [CrossRef]
6. Wu, C.; Li, Y.K.; Wan, C.L. Reactive-sintering B_4C matrix composite for Armor Applications. *Rare Met.* **2020**, *39*, 529–544. [CrossRef]
7. Huang, S.G.; Vanmeensel, K.; van der Biest, O.; Vleugels, J. In situ synthesis and densification of submicormeter-grained B_4C-TiB_2 composites by pulsed electric current sintering. *J. Eur. Ceram. Soc.* **2011**, *31*, 637–644. [CrossRef]
8. Xu, C.M.; Cai, Y.B.; Flodstrom, K.; Li, Z.; Esmaeilzadeh, S.; Zhang, G.J. Spark plasma sintering of B_4C ceramics: The effects of milling medium and TiB_2 addition. *Int. Refract. Met. Hard Mater.* **2012**, *30*, 139–144. [CrossRef]
9. Goldstein, A.; Geffen, Y.; Goldenberg, A. Boron Carbide–Zirconium Boride In-Situ Composites by the Reactive Pressureless Sintering of Boron Carbide–Zirconia Mixtures. *J. Am. Ceram. Soc.* **2001**, *84*, 642–644. [CrossRef]
10. Subramanian, C.; Roy, T.; Murthy, T.S.; Sengupta, P.; Kale, G.B.; Krishnaiah, M.V.; Suri, A.K. Effect of zirconia addition on pressureless sintering of boron carbide. *Ceram. Int.* **2008**, *34*, 1543–1549. [CrossRef]
11. Sairam, K.; Sonber, J.K.; Murthy, T.S.; Subramanian, C.; Hubli, R.C.; Suri, A.K. Development of B_4C–HfB_2 composites by reaction hot pressing. *Int. Refract. Met. Hard Mater.* **2012**, *35*, 32–40. [CrossRef]
12. Tang, J.; Tan, S.H.; Chen, Z.M.; Jiang, D.L. Strengthening and Toughening of B_4C-TiB_2 Multiphase Ceramics. *J. Inorg. Mater.* **1997**, *12*, 169–174. [CrossRef]
13. Nils, C.; Bernhard, M.; Michael, V.S. Grain-Size dependence of fracture energy in ceramics. *J. Am. Ceram. Soc.* **1981**, *64*, 345–350. [CrossRef]
14. Liu, Z.; Wang, D.; Li, J.; Huang, Q.; Ran, S. Densification of high-strength B_4C–TiB_2 composites fabricated by pulsed electric current sintering of TiC–B mixture. *Scr. Mater.* **2017**, *135*, 15–18. [CrossRef]
15. Wang, D.; Ran, S.; Shen, L.; Sun, H.; Huang, Q. Fast synthesis of B_4C–TiB_2 composite powders by pulsed electric current heating TiC–B mixture. *J. Eur. Ceram. Soc.* **2015**, *35*, 1107–1112. [CrossRef]
16. Huang, S.G.; Vanmeensel, K.; Malek, O.J.A.; Van der Biest, O.; Vleugels, J. Microstructure and mechanical properties of pulsed electric current sintered B_4C–TiB_2 composites. *Mater. Sci. Eng. A* **2011**, *528*, 1302–1309. [CrossRef]
17. Wu, C.; Li, Y.K. AlN-induced reinforcement of nano-amorphous B-C-N compound for TiB_2–B_4C ceramic composite. *J. Alloys Compd.* **2020**, *831*, 154074. [CrossRef]
18. Mashhadi, M.; Taheri-Nassaj, E.; Mashhadi, M.; Sglavo, V.M. Pressureless sintering of B_4C–TiB_2 composites with al additions. *Ceram. Int.* **2011**, *37*, 3229–3235. [CrossRef]
19. Malek, O.; Vleugels, J.; Vanmeensel, K.; Huang, S.; Liu, J.; Van den Berghe, S.; Datye, A.; Wu, K.H.; Lauwers, B. Electrical discharge machining of B_4C–TiB_2 composites. *J. Eur. Ceram. Soc.* **2011**, *31*, 2023–2030. [CrossRef]
20. Goldstein, A.; Yeshurun, Y.; Goldenberg, A. B_4C/metal boride composites derived from B_4C/metal oxide mixtures. *J. Eur. Ceram. Soc.* **2007**, *27*, 695–700. [CrossRef]
21. Yamada, S.; Hirao, K.; Yamauchi, Y.; Kanzaki, S. High strength B_4C–TiB_2 composites fabricated by reaction hot-pressing. *J. Eur. Ceram. Soc.* **2003**, *23*, 1123–1130. [CrossRef]
22. Liu, Z.T.; Deng, X.G.; Li, J.M.; Sun, Y.; Ran, S. Effects of B_4C particle size on the microstructures and mechanical properties of hot-pressed B_4C-TiB_2 composites. *Ceram. Int.* **2018**, *44*, 21415–21420. [CrossRef]
23. Li, P.; Yang, J.F. Microstructure and Mechanical Properites of B_4C-C Ceramic. *Rare Met. Mater. Eng.* **1999**, *28*, 151–154.
24. Suri, A.K.; Subramanian, C.; Sonber, J.K.; Murthy, T.C. Synthesis and consolidation of boron carbide: A review. *Int. Mater. Rev.* **2010**, *55*, 4–40. [CrossRef]
25. Hayun, S.; Frage, N.; Dariel, M.P. The morphology of ceramic phases in B_xC-SiC-Si infiltrated composites. *J. Solid State Chem.* **2006**, *179*, 2875–2879. [CrossRef]
26. Feng, Y.; Hou, Z.; Zhang, H.; Liu, L. Densification and Mechanical Properties of Spark Plasma Sintered B_4C with Si as a Sintering Aid. *J. Am. Ceram. Soc.* **2010**, *93*, 2956–2959. [CrossRef]
27. Zhang, Z.; Du, X.; Li, Z.; Wang, W.; Zhang, J.; Fu, Z. Microstructures and mechanical properties of B_4C-SiC intergranular/intragranular nanocomposite ceramics fabricated from B_4C, Si, and graphite powders. *J. Eur. Ceram. Soc.* **2014**, *34*, 2153–2161. [CrossRef]
28. Skorokhod, V.V., Jr.; Vlajic, M.D.; Kristic, V.D. Pressureless Sintering of B_4C-TiB_2 Ceramic Composites. *Mater. Sci. Forum* **1998**, *282–283*, 219–224. [CrossRef]
29. Baharvandi, H.R.; Hadian, A.M. Pressureless Sintering of TiB_2-B_4C Ceramic Matrix Composite. *J. Mater. Eng. Perform.* **2008**, *17*, 838–841. [CrossRef]
30. Pan, J.S.; Tong, J.M.; Tian, M.B. *Fundamentals of Materials Science*; Tsinghua University Press: Beijing, China, 2011.
31. Mu, B.C. *Strengthening and Toughening of Ceramic Materials*; Metallurgical Industry Press Co., Ltd.: Beijing, China, 2002.
32. Choi, S.R.; Sanders, W.A.; Salem, J.A.; Tikare, V. Young's modulus, strength and fracture toughness as a function of density of in situ toughened silicon nitride with 4 wt.% Scandia. *J. Mater. Sci. Lett.* **1995**, *14*, 276–278. [CrossRef]
33. Li, Z.N. *Applied Fracture Mechanics*; Bei Hang University Press: Beijing, China, 2012.
34. Wu, Q.R.; Wen, B.X. Study on temperature dependence of thermal conductivity and linear expansion for SiC material. *J. South China Univ. Technol. Nat. Sci. Ed.* **1996**, *24*, 11–15.
35. Einarsrud, M.A.; Hagen, E.; Pettersen, G.; Grande, T. Pressureless sintering of titanium diboride with nickel, nickel boride, and iron additives. *J. Am. Ceram. Soc.* **2005**, *80*, 3013–3020. [CrossRef]